

# Targeted Functionalization of Cyclic Ether Solvents for Controlled Reactivity in High-Voltage Lithium Metal Batteries

Yan Zhao,<sup>‡</sup> Tianhong Zhou,<sup>‡</sup> Dominika Baster, Mario El Kazzi, Jang Wook Choi,\* and Ali Coskun\*



Cite This: *ACS Energy Lett.* 2023, 8, 3180–3187



Read Online

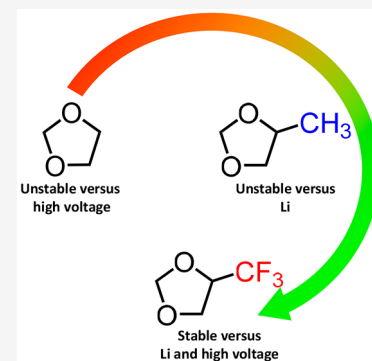
ACCESS |

Metrics & More

Article Recommendations

Supporting Information

**ABSTRACT:** Understanding the degradation pathways and reactivity of electrolytes is the key to address the shortcomings of conventional electrolytes and to develop new electrolytes for high-voltage lithium metal batteries (LMBs). Accordingly, while 1,3-dioxolane (DOL) exhibits desired features such as good compatibility with Li metal, low viscosity, and high ionic conductivity, it suffers from poor oxidation stability, mainly from its ring-opening polymerization. In an effort to control the reactivity of DOL by tuning its electronic properties, we introduced methyl and trifluoromethyl groups to the ethyl moiety of DOL and developed 4-methyl-1,3-dioxolane (MDOL) and 4-(trifluoromethyl)-1,3-dioxolane (TFDOL) as solvents, respectively. Whereas the MDOL-based electrolyte exhibited serious side reactions toward metallic Li, the TFDOL-based electrolyte showed oxidation stability up to 5.0 V. Moreover, the inorganic-rich solid electrolyte interphase induced by the weak solvation power of TFDOL along with high oxidation stability enabled a robust cycling stability in a Li/LiNCM811 full cell (20  $\mu$ m Li foil, N/P ratio of 2.5).



**D**riving range constraints of electric vehicles (EVs) originate from the limited energy density of conventional lithium ion batteries (LIBs).<sup>1,2</sup> Lithium metal batteries (LMBs), adopting a lithium metal anode as an alternative to graphite, have been recognized to achieve far superior energy density close to 500 Wh kg<sup>-1</sup>.<sup>3–7</sup> However, LMBs suffer from poor cycle life and safety issues owing to uncontrollable side reactions between the Li metal anode and electrolyte, ascribed to the low thermodynamic stability of electrolytes toward metallic Li. The resulting unstable interface leads to the formation of a mechanically fragile solid electrolyte interphase (SEI), which induces unwanted Li dendrite growth and “dead” Li. These individual phenomena are inter-related, giving rise to negative effects on each other during cycling.<sup>8,9</sup>

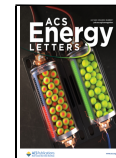
Since it was noted that the unstable SEI is rooted in incompatible electrolyte compositions, there have been significant research efforts to develop and optimize electrolyte components. Manipulating solvation structure, and thereby controlling the SEI chemistry, is one of the most effective approaches along this direction.<sup>10</sup> Several strategies involving the use of high-concentration electrolytes,<sup>11–15</sup> localized high-concentration electrolytes,<sup>16–22</sup> additives,<sup>23–25</sup> and new solvents<sup>26–31</sup> have been reported to improve the cyclability of LMBs to some extent. As for the traditional electrolytes, mainly consisting of carbonates and ethers, there are obvious limitations with respect to their compatibility with Li metal

anode and oxidation stability, respectively.<sup>32</sup> Compared to the carbonate electrolytes, ether-based electrolytes such as 1,2-dimethoxyethane (DME) and 1,3-dioxolane (DOL) result in flat and large Li grains during plating which decrease the contact area between the electrolyte and plated Li to realize higher Coulombic efficiency (CE).<sup>33</sup> The limited oxidation stability (<4 V) of ether-based electrolytes, however, constrains their application in high-voltage LMBs when paired with high-Ni layered cathodes. For example, adopting the *in situ* polymerization of DOL in the DOL/DME mixture using a Lewis acid initiator shows a clear increase of the electrochemical window,<sup>34,35</sup> which hints that the electrochemical ring-opening polymerization is responsible for the poor oxidation stability of DOL. Accordingly, targeted functionalization of the molecular structure of DOL could be an efficient strategy to control its reactivity and to mitigate ring-opening polymerization, thus enabling new solvents suitable for high-voltage LMBs.<sup>36</sup>

Received: May 22, 2023

Accepted: June 15, 2023

Published: June 27, 2023



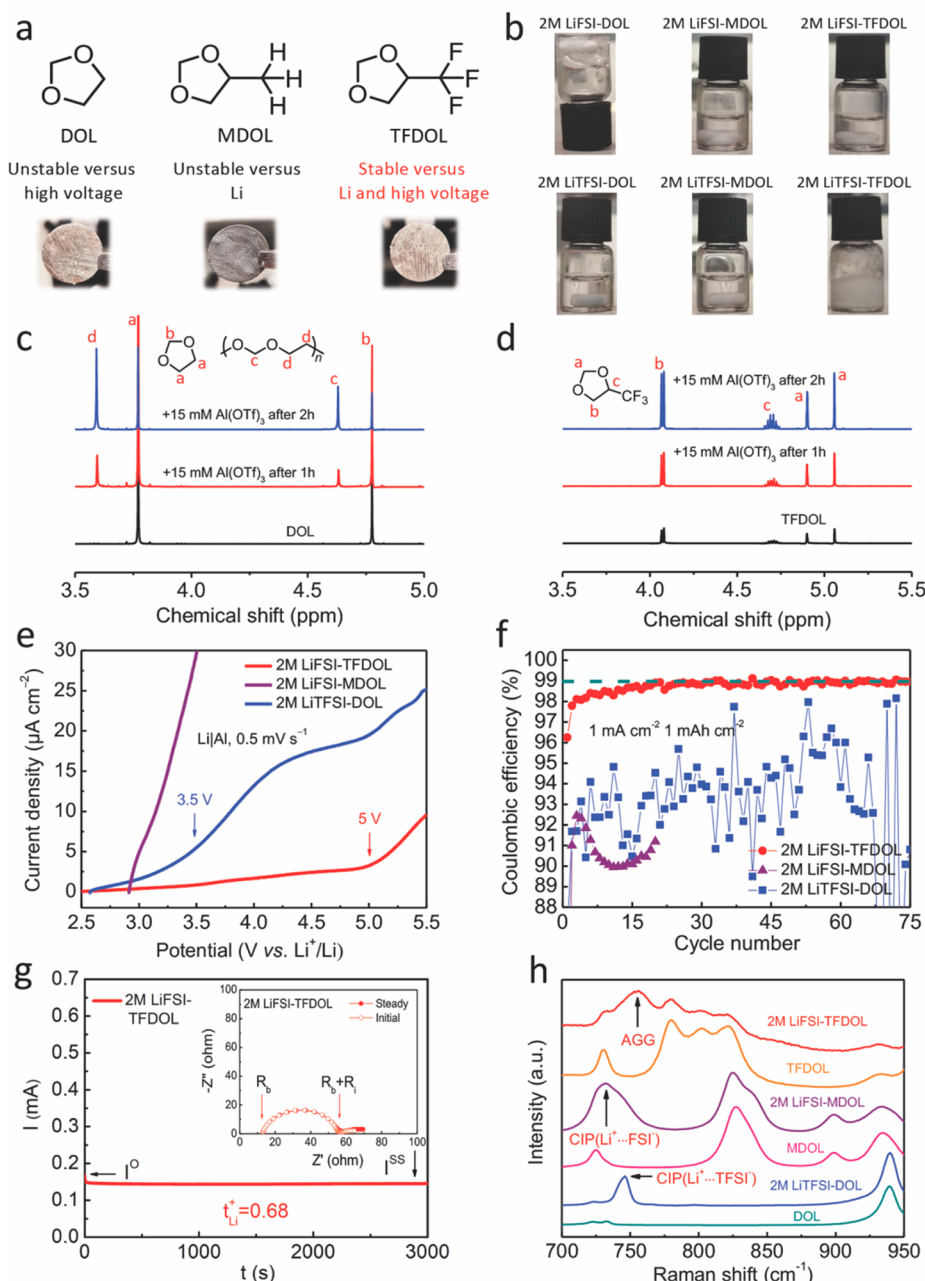


**Figure 1.** (a) Molecular structures and properties of the solvents, namely, DOL, MDOL, and TFDOL, along with the optical images of polished Li soaked in the solvents for 10 min. (b) Optical images of 2 M LiFSI-DOL (gel state), 2 M LiFSI-MDOL, 2 M LiFSI-TFDOL, 2 M LiTFSI-DOL, 2 M LiTFSI-MDOL, and 2 M LiTFSI-TFDOL (insoluble state). (c, d) <sup>1</sup>H NMR spectra ( $\text{DMSO}-d_6$ ) of liquid DOL and TFDOL without or with  $\text{Al}(\text{OTf})_3$  initiator at 1 and 2 h. (e) Oxidation stability of electrolytes in Li|Al half cells obtained from LSV. (f) Coulombic efficiencies (CEs) for the first 75 cycles in the 2 M LiTFSI-DOL, 2 M LiFSI-MDOL, and 2 M LiFSI-TFDOL electrolytes at 1 mA  $\text{cm}^{-2}$  current density with 1 mAh  $\text{cm}^{-2}$  Li. (g) Chronoamperometry profile of the Li|TFDOL electrolyte|Li cell under a polarization voltage of 10 mV, and the corresponding EIS profiles before and after polarization (inset). (h) Raman spectra of various electrolytes.

Having recognized the critical role of O atoms in the ring-opening polymerization reaction, in the work described herein we modified the structure and electronic properties of DOL by integrating electron-donating methyl and electron-withdrawing trifluoromethyl groups to form 4-methyl-1,3-dioxolane (MDOL) and 4-(trifluoromethyl)-1,3-dioxolane (TFDOL), respectively. MDOL exhibited serious side reactions toward Li metal owing to the higher electron density of the O atoms,<sup>37</sup> which limits its application toward LMBs. After the 2 M lithium bis(fluorosulfonyl)imide (LiFSI) salt was dissolved, the

resulting 2 M LiFSI-TFDOL liquid electrolyte showed excellent oxidation stability up to 5 V, originating from the electron-withdrawing  $-\text{CF}_3$  group that hinders the ring-opening polymerization, unlike DOL-based gel electrolyte at the same salt concentration (2 M LiFSI-DOL). Moreover, TFDOL solvent enhanced the coordination between  $\text{Li}^+$  and  $\text{FSI}^-$  ions, which promoted the formation of an anion-derived, stable SEI layer and realized highly reversible Li plating/stripping. Based on the enhanced compatibility with the Li metal anode and the wide electrochemical window of 2 M

LiFSI-TFDOL, limited-excess Li|LiNi<sub>0.8</sub>Co<sub>0.1</sub>Mn<sub>0.1</sub>O<sub>2</sub> (NCM811) full cells realized 89% retention after 100 cycles at 1 C; more importantly, the full cell using 2 M LiFSI-TFDOL-SDME exhibited 94.5% retention at 1 C after 220 cycles, thus demonstrating the pivotal role of functional groups to control the reactivity and performance of cyclic ether-based electrolytes.

The origin of the low oxidation stability of DOL is the ring-opening polymerization, which makes DOL's application infeasible for high-voltage LMBs.<sup>34,35</sup> On the other hand, tuning the molecular structure of ethers through targeted functionalization offers enormous potential as a reliable strategy for next-generation LMBs. In an effort to control the electronic properties and thus the reactivity of DOL, we opted to attach an electron-donating -CH<sub>3</sub> group and an electron-withdrawing -CF<sub>3</sub> group to the ethyl moiety of DOL to obtain so-called MDOL and TFDOL solvents, respectively (Figure 1a). First, the polished Li discs were soaked in DOL, MDOL, and TFDOL to check their chemical compatibility with metallic Li. MDOL exhibited serious side reactions toward Li metal, evidenced by the dark surface, presumably due to the increased donicity of the O atoms, whereas there was no obvious change with both DOL and TFDOL, implying that, contrary to MDOL bearing an electron-donating group, TFDOL with the electron-withdrawing group maintains chemical stability with metallic Li. Based on these initial results, DOL and TFDOL were selected for further study. Upon dissolution of the 2 M LiFSI salt in DOL, LiFSI triggers ring-opening polymerization of DOL and transforms a liquid DOL-based electrolyte to a gel state. In stark contrast, TFDOL can dissolve 2 M LiFSI in a transparent liquid state. In addition, when dissolving 2 M LiTFSI, TFDOL formed a suspension which originated from its weakened solvation power, while DOL maintained the liquid state and formed a clear solution at the same LiTFSI salt concentration (Figure 1b). Therefore, 2 M LiTFSI-DOL and 2 M LiTFSI-TFDOL liquid electrolytes were selected for comparative analysis in high-voltage LMBs. Proton nuclear magnetic resonance (<sup>1</sup>H NMR) spectroscopy was carried out to probe the reactivities of DOL and TFDOL toward ring-opening polymerization in the presence of a Lewis acid, Al(OTf)<sub>3</sub> (Figure 1c,d). Upon addition of 15.0 mM Al(OTf)<sub>3</sub> initiator, whereas no new peaks were observed in the case of TFDOL even after 2 h, new peaks emerged in DOL after 1 h, which was attributed to the formation poly-DOL,<sup>34</sup> and the ratio of poly-DOL to DOL increased after 2 h. This result revealed the higher stability of TFDOL toward ring-opening polymerization.

TFDOL was synthesized in one step by reacting 1,1,1-trifluoro-2,3-propanediol<sup>38</sup> with paraformaldehyde at room temperature for 1 h in 95% sulfuric acid, with 35% yield (Figure S1). The formation of TFDOL was confirmed by NMR spectroscopy analysis (Figures S1 and S2). The 2 M LiTFSI-DOL and 2 M LiTFSI-TFDOL electrolytes showed ionic conductivity values of 13.2 and 3.7 mS cm<sup>-1</sup> at 25 °C, respectively. The physicochemical properties of DOL and TFDOL solvents and the corresponding electrolytes are further summarized in Table S1. Linear sweep voltammetry (LSV) measurements were performed on LiAl half-cells to determine the oxidation stability of the 2 M LiTFSI-DOL, 2 M LiTFSI-MDOL, and 2 M LiTFSI-TFDOL electrolytes. Compared to the low oxidation voltage of 2 M LiTFSI-DOL (~3.5 V), 2 M LiTFSI-MDOL showed even worse anodic stability due to the existence of the weakly electron-donating group, whereas the

oxidation tolerance of 2 M LiFSI-TFDOL was extended to 5 V (Figure 1e). The oxidation stability of the electrolytes was also evaluated by analyzing the Li|SuperP + PVDF@CP half-cells (Figure S3). This result points to the effect of rational functionalization of DOL with regard to the electrochemical stability window by suppressing its ring-opening. In agreement with the LSV result, TFDOL exhibited a much lower highest occupied molecular orbital (HOMO) energy level (-8.09 eV) compared to that of DOL (-7.23 eV) (Figure S4) due to the electron-withdrawing -CF<sub>3</sub> group.<sup>39</sup>

The CEs of Li|Cu cells with different electrolytes were tested at a current density of 1 mA cm<sup>-2</sup> with an areal capacity of 1 mAh cm<sup>-2</sup> to evaluate the reversibility of Li stripping/plating. The inferior reversibility of 2 M LiTFSI-DOL was quite clear from the beginning of cycling. The 2 M LiFSI-MDOL electrolyte also presented a limited average CE of only 90.1% after 20 cycles. By contrast, 2 M LiFSI-TFDOL showed a more steady CE of ~99.0% for the first 75 cycles (Figure 1f) with smooth Li stripping/plating profiles (Figure S5). Also, the average CE of 98.5% was maintained for over 120 cycles at a current density of 1 mA cm<sup>-2</sup> with a capacity of 1 mAh cm<sup>-2</sup> (Figure S6), indicating that the trifluoromethylation did not compromise the decent Li stripping/plating behavior. Consistent with this, cyclic voltammetry (CV) of the 2 M LiFSI-MDOL electrolyte showed a poor reversibility in Li plating/stripping with obvious side reaction peaks, originating from the continuous reaction between Li metal and MDOL (Figure S7), in agreement with the appearance of the black Li surface after soaking in MDOL, as shown in Figure 1a. We also assembled Li|Li symmetrical cells with the 2 M LiTFSI-DOL and 2 M LiTFSI-TFDOL electrolytes (Figure S8). The voltage polarization of the cell with 2 M LiTFSI-DOL began to increase sharply after 155 h, while the cell with the 2 M LiTFSI-TFDOL electrolyte could continue the cycling over 460 h at a current density of 1 mA cm<sup>-2</sup> with an areal capacity of 1 mAh cm<sup>-2</sup>, implying stable Li deposition and dissolution at the Li metal interface. The Li ion transference number (LTN) is another vital parameter for the electrolytes in LMBs.<sup>40</sup> A higher LTN (0.68) was achieved for 2 M LiFSI-TFDOL, compared to that of 2 M LiTFSI-DOL (0.53) (Figures 1g and S9), possibly resulting from the weak solvation power of TFDOL that promotes the coordination between Li<sup>+</sup> and the FSI anion.

To elucidate the solvation structure of the electrolytes, Raman spectroscopy analysis was carried out for the 2 M LiTFSI-DOL, 2 M LiTFSI-MDOL, and 2 M LiTFSI-TFDOL electrolytes (Figure 1h). In the case of the 2 M LiTFSI-DOL and 2 M LiTFSI-MDOL electrolytes, the majority of anions existed as contact-ion pairs (CIPs, with an anion coordinating to one Li<sup>+</sup>) (746 cm<sup>-1</sup> for TFSI anion,<sup>41</sup> 732.5 cm<sup>-1</sup> for FSI anion<sup>42</sup>). Unlike DOL- and MDOL-based electrolytes, in the case of the 2 M LiTFSI-TFDOL electrolyte, most of the anions remained in an aggregate state (AGG, with an anion coordinating to two or more Li<sup>+</sup>) (755 cm<sup>-1</sup>).<sup>43</sup> This difference endowed TFDOL with a relatively weak solvation power to induce an anion-derived SEI composition. These findings were also further verified by electrostatic potential (ESP) calculations (Figure S10). The decreased electron density of the -O- atom in the TFDOL solvent leads to a weaker solvation power compared to the DOL solvent, which is once again ascribed to the targeted functionalization with the electron-withdrawing nature of the -CF<sub>3</sub> functional group.<sup>30</sup>

The morphologies of Li were visualized by scanning electron microscopy (SEM). First, 2 mAh cm<sup>-2</sup> Li was deposited at 1

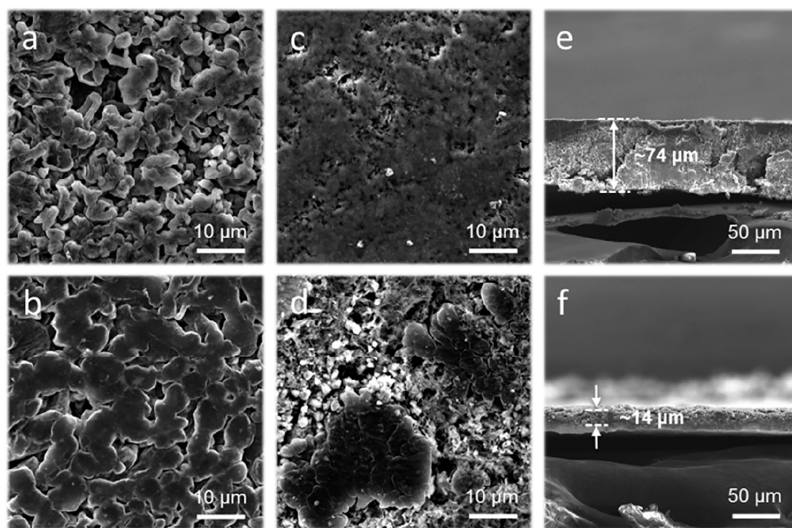


**Figure 2.** (a, b) SEM images of  $2 \text{ mAh cm}^{-2}$  Li plating morphology at  $1 \text{ mA cm}^{-2}$  in (a) 2 M LiTFSI-DOL and (b) 2 M LiFSI-TFDOL electrolytes. (c, d) Morphology of Li after 30 cycles at  $1 \text{ mA cm}^{-2}$  with a cutoff capacity of  $1 \text{ mAh cm}^{-2}$  in (c) 2 M LiTFSI-DOL and (d) 2 M LiFSI-TFDOL electrolytes. (e, f) Cross-sectional view SEM images of Li on a Cu substrate in (e) 2 M LiTFSI-DOL and (f) 2 M LiFSI-TFDOL electrolytes.

$\text{mA cm}^{-2}$  in Li|Cu half cells with different electrolytes. A loose surface with a small grain size and an irregular Li growth was observed in the 2 M LiTFSI-DOL cell (**Figures 2a** and **S11a**), while the surface of the electrodeposited Li in the 2 M LiFSI-TFDOL cell remained visibly compact, uniform, and flat (**Figures 2b** and **S11b**). In order to investigate the morphology evolution of Li after cycling, Li|Cu half cells were disassembled after 30 cycles at  $1 \text{ mA cm}^{-2}$  with a cutoff capacity of  $1 \text{ mAh cm}^{-2}$ . The 2 M LiTFSI-DOL cell showed a very thick SEI film on the surface of the Li metal (**Figures 2c** and **S11c**). In contrast, large and clean Li grains were observed in the 2 M LiFSI-TFDOL cell, reflecting an improved interfacial stability of the 2 M LiFSI-TFDOL electrolyte with the Li metal anode (**Figures 2d** and **S11d**). In connection with the lower CE and uneven Li deposition, the 2 M LiTFSI-DOL cell showed a very thick Li layer, with a thickness of  $74 \mu\text{m}$  after 30 cycles (**Figure 2e**). On the contrary, after the same number of cycles, a very thin Li layer of only  $14 \mu\text{m}$  was observed in the 2 M LiFSI-TFDOL cell where plated Li closely contacts (**Figure 2f**), pointing out its homogeneous electrochemical plating and stripping process over repeated cycling.

CV was conducted to further study the stability of the Li plating/stripping behavior (**Figure S12**). 2 M LiFSI-TFDOL showed higher reversibility compared with 2 M LiTFSI-DOL, which is line with the superior cycle life of 2 M LiFSI-TFDOL. Electrochemical impedance spectroscopy (EIS) was carried out to investigate the interfacial kinetics of the Li metal electrode after 1 cycle and 20 cycles at  $1 \text{ mA cm}^{-2}$  with  $1 \text{ mAh cm}^{-2}$  in a Li|Cu half-cell configuration (**Figure S13**). After 20 cycles, an increased charge-transfer resistance ( $R_{ct}$ ) was observed for 2 M LiTFSI-DOL, whereas 2 M LiFSI-TFDOL maintained a stable  $R_{ct}$  over time, indicating that TFDOL induced an interface that effectively maintained Li-ion transport on the Li metal during cycling.

NCM811 full cells with different electrolytes were evaluated to determine the effect of functionalization in a practical cell setting. We used a  $20 \mu\text{m}$  Li foil as the anode (N/P ratio of 2.5) for these full cells and cycled them at a high rate of 1 C ( $1 \text{ C} = 200 \text{ mA g}^{-1}$ ) in both charge and discharge with a

voltage range of 3–4.4 V (**Figure 3a,b**). Due to the serious side reaction toward Li metal, the 2 M LiFSI-MDOL electrolyte could be cycled for only 10 cycles before a sudden failure occurred. Remarkably, the Li|NCM811 full cell with the 2 M LiFSI-TFDOL electrolyte delivered an outstanding cycling performance up to 100 cycles with a specific capacity of  $147 \text{ mA h g}^{-1}$  and a capacity retention of 89.0% at 1 C, which is remarkable considering that the system was tested as a single solvent without any additives. Electrolytes with different salt concentrations were also compared (**Figure S14**). The H<sub>2</sub>–H<sub>3</sub> phase transformation is the crucial cause of the delay of discharge voltage and capacity of NCM811.<sup>44</sup> Even after 100 cycles, the H<sub>2</sub>-H<sub>3</sub> peak still existed, demonstrating the outstanding cathodic stability in the 2 M LiFSI-TFDOL electrolyte (**Figure S15**).<sup>45</sup> In contrast, the 2 M LiTFSI-DOL electrolyte decayed severely within 20 cycles, and the performance of the LiTFSI-based electrolyte with the DOL-DME mixture was also compared (**Figure S16**). In addition, the 1 M LiPF<sub>6</sub>-EC-EMC carbonate-based electrolyte exhibited fast capacity fade, with a specific capacity of only  $115.7 \text{ mA h g}^{-1}$  retained after 50 cycles (**Figure 3c**). In order to further improve the electrolyte performance of full cells, TFDOL was mixed with DME in different volume ratios (**Figures 3d,e** and **S17**). The cell using 2 M LiFSI-STFDOL-SDME showed the most stable CE in Li|Cu half cells compared with the other mixtures (**Figure S17**). More importantly, the full cell using 2 M LiFSI-STFDOL-SDME exhibited 94.5% retention at 1 C after 220 cycles. This obvious improvement in cycling performance compared to the cells using 2 M LiFSI-SDOL-SDME and 2 M LiFSI-DME revealed the advantage of TFDOL itself (**Figure 3d**). Moreover, even under extremely harsh conditions of an N/P ratio of 1.0 and an ultrahigh loading of  $20 \text{ mg cm}^{-2}$ , the full cell using the 2 M LiFSI-SDOL-SDME electrolyte could keep 95.9% retention after 100 cycles (**Figure 3e**). Performance comparisons of full cells support the competitiveness of the TFDOL-based electrolyte (**Table S2**).

X-ray photoelectron spectroscopy (XPS) analysis was conducted to systematically probe the SEI (**Figure S18**) and

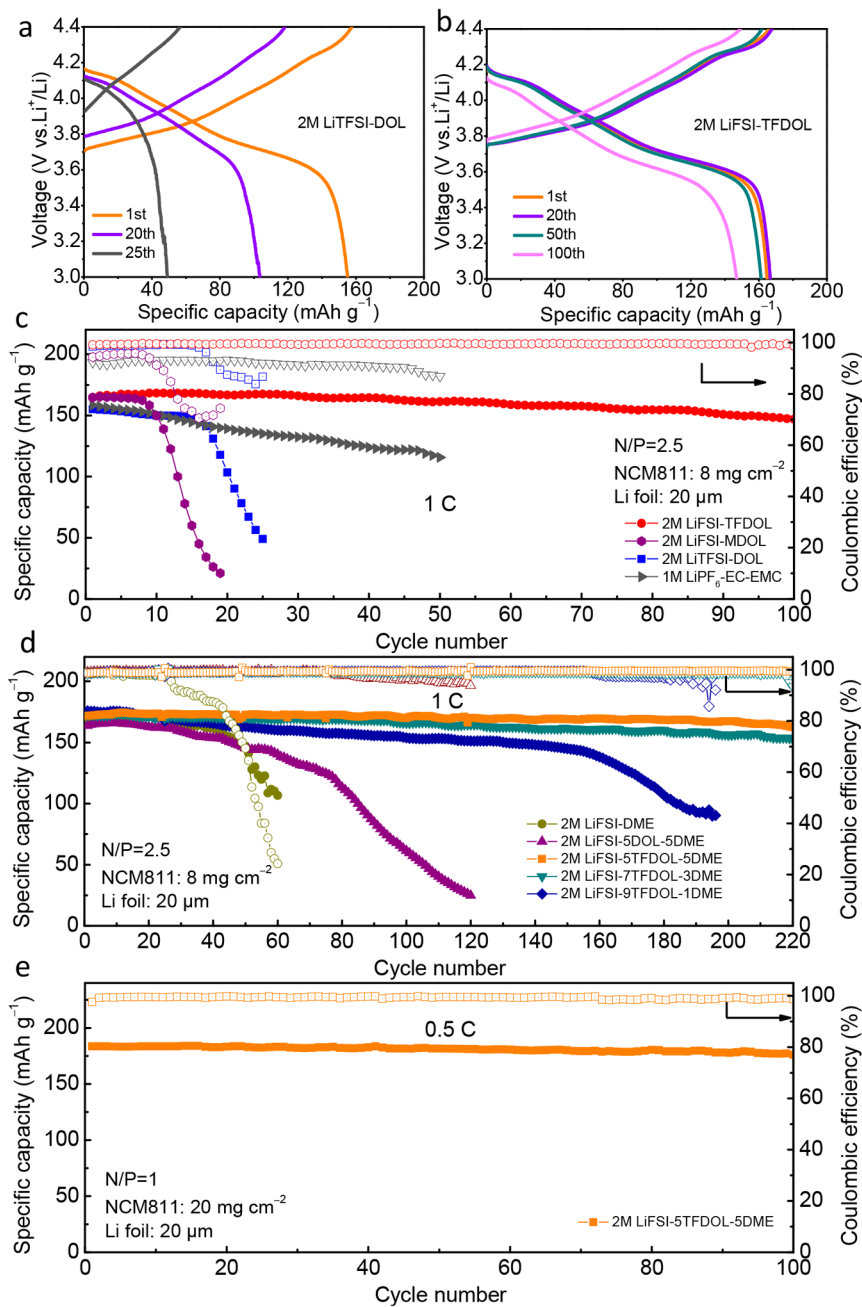


**Figure 3.** (a, b) Galvanostatic discharge–charge profiles of Li|NCM811 full cells at 1 C in (a) 2 M LiTFSI-DOL and (b) 2 M LiFSI-TFDOL electrolytes. (c) Cycling performance and CEs at 1 C of Li|NCM811 full cells with different electrolytes. (d) Cycling performance of Li|NCM811 full cells at 1 C with different solvent mixtures. (e) Performance of high-loading Li|NCM811 full cell at 0.5 C with TFDOL-based electrolyte with an N/P ratio of 1.0. All Li foil thicknesses are 20  $\mu\text{m}$ , 1 C = 200  $\text{mA g}^{-1}$ .

cathode electrolyte interphase (CEI) (Figure S19) compositions in Li|NCM811 full cells after 20 cycles at 1 C. In C 1s spectra (Figure 4a–c), SEI in the 2 M LiFSI-TFDOL cell showed a  $\text{CF}_3$  peak (292.9 eV), indicating that TFDOL participated in forming the SEI.<sup>16</sup> The weaker C–C–O peak (286.5 eV) observed from the 2 M LiFSI-TFDOL cell demonstrated weaker side reactions of TFDOL toward the Li anode compared to the 2 M LiTFSI-DOL and 2 M LiFSI-MDOL electrolytes.<sup>12</sup> In the F 1s spectra (Figure 4d–f), the stronger S–F signal (688.1 eV) in the case of the 2 M LiFSI-TFDOL electrolyte indicated more FSI anion participation in the SEI formation.<sup>46,47</sup> In the S 2p spectra (Figure S20), an

obvious  $\text{S}_n^{2-}$  peak (161.5 eV, 162.3 eV) was observed for the 2 M LiFSI-TFDOL cell, while it did not appear for the 2 M LiFSI-MDOL cell, indicating that LiFSI was more seriously reduced in the 2 M LiFSI-TFDOL cell.<sup>16</sup> Meanwhile, the low intensity of the  $\text{S}_n^{2-}$  peak in the 2 M LiTFSI-DOL cell revealed the weak decomposition of LiTFSI. Notably, in C 1s spectra (Figure 4g–i), the CEI from the 2 M LiTFSI-DOL cell presented an extremely high C–O (286.5 eV) peak, which is ascribed to the serious ring-opening polymerization of DOL, while the peak largely weakened in the 2 M LiFSI-TFDOL cell, verifying the significantly suppressed solvent decomposition.<sup>12,48</sup> In addition, a new  $-\text{CF}_3$  peak at 292.9 eV was

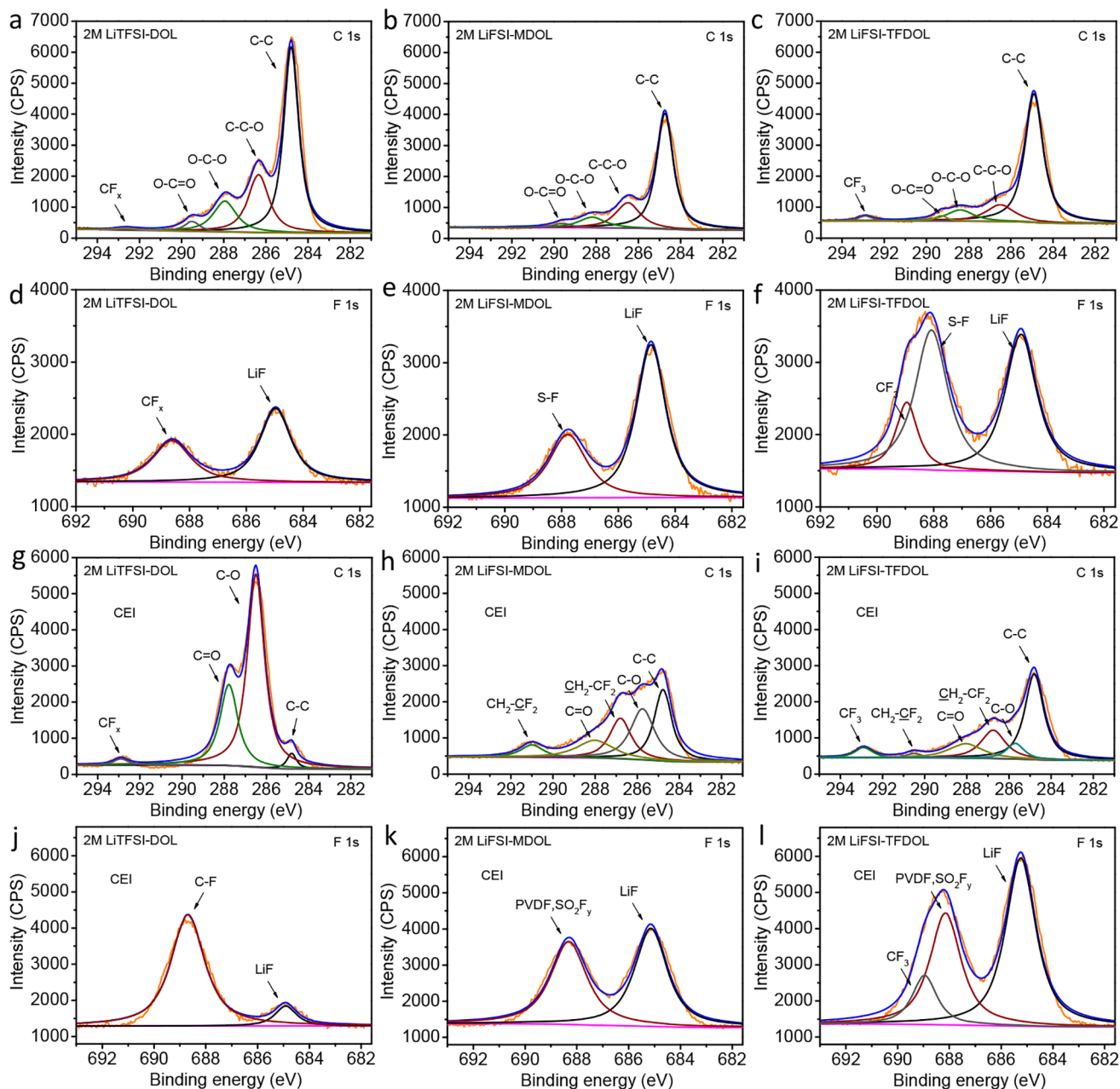


**Figure 4.** (a–f) C 1s and F 1s XPS profiles of SEI in Li|NCM811 full cells with (a, d) 2 M LiTFSI-DOL, (b, e) 2 M LiFSI-MDOL, and (c, f) 2 M LiFSI-TFDOL electrolytes. (g–l) C 1s and F 1s XPS profiles of CEI in Li|NCM811 full cells with (g, j) 2 M LiTFSI-DOL, (h, k) 2 M LiFSI-MDOL, and (i, l) 2 M LiFSI-TFDOL electrolytes after 20 cycles at 1 C.

observed on the NCM811 cathode surface, suggesting the participation of TFDOL in the formation of the CEI film on the NCM811 cathode surface.<sup>49</sup> In F 1s spectra (Figure 4j–l), the LiF-rich character of CEI was revealed in 2 M LiFSI-TFDOL compared with 2 M LiFSI-MDOL. Meanwhile, the weakened LiF peak of 2 M LiTFSI-DOL resulted from weak decomposition of LiTFSI. CEIs of cathodes in Li|NCM811 full cells with various electrolytes were also examined by transmission electron microscopy (TEM) after 20 cycles at 1 C (Figure S21). Compared with the 2 M LiTFSI-DOL and 2 M LiFSI-MDOL cells, the 2 M LiFSI-TFDOL cell presented a thinner and more homogeneous CEI layer. Through our targeted functionalization approach to control the reactivity of DOL, a new single cyclic ether solvent was introduced and

successfully paired with the otherwise incompatible LiFSI salt, which realized excellent electrochemical performance in the high-voltage LMBs.

In summary, we demonstrated the targeted functionalization of a cyclic ether with a trifluoromethyl moiety to manipulate its physical, chemical, and electrochemical properties to meet the demands on both anode and cathode sides as a single solvent for high-voltage LMBs. Trifluoromethylation not only suppressed ring-opening polymerization to realize excellent antioxidation ascribed to the strong electron-withdrawing effect, but also led to robust cycling performance in both Li|Cu half cell and Li|NCM811 full cell configurations. The functionalization of solvents to block interfacial degradation

cascades offers a promising pathway for the development of new ether solvents for practical lithium metal batteries.

## ■ ASSOCIATED CONTENT

### SI Supporting Information

The Supporting Information is available free of charge at <https://pubs.acs.org/doi/10.1021/acsenergylett.3c01004>.

Experimental details, NMR spectra, electrolyte properties, CE profiles, voltage–time profiles, CV, EIS, XPS, and TEM images ([PDF](#))

## ■ AUTHOR INFORMATION

### Corresponding Authors

Ali Coskun – Department of Chemistry, University of Fribourg, Fribourg 1700, Switzerland;  [orcid.org/0000-0002-4760-1546](https://orcid.org/0000-0002-4760-1546); Email: [ali.coskun@unifr.ch](mailto:ali.coskun@unifr.ch)

Jang Wook Choi – School of Chemical and Biological Engineering, Department of Materials Science and Engineering, and Institute of Chemical Processes, Seoul National University, Gwanak-gu, Seoul 08826, Republic of Korea;  [orcid.org/0000-0001-8783-0901](https://orcid.org/0000-0001-8783-0901); Email: [jangwookchoi@snu.ac.kr](mailto:jangwookchoi@snu.ac.kr)

### Authors

Yan Zhao – Department of Chemistry, University of Fribourg, Fribourg 1700, Switzerland;  [orcid.org/0000-0001-5324-5050](https://orcid.org/0000-0001-5324-5050)

Tianhong Zhou – Department of Chemistry, University of Fribourg, Fribourg 1700, Switzerland;  [orcid.org/0000-0002-9537-8465](https://orcid.org/0000-0002-9537-8465)

Dominika Baster – Electrochemistry Laboratory, Paul Scherrer Institut, Villigen 5232, Switzerland;  [orcid.org/0000-0002-6732-0565](https://orcid.org/0000-0002-6732-0565)

Mario El Kazzi – Electrochemistry Laboratory, Paul Scherrer Institut, Villigen 5232, Switzerland;  [orcid.org/0000-0003-2975-0481](https://orcid.org/0000-0003-2975-0481)

Complete contact information is available at:

<https://pubs.acs.org/10.1021/acsenergylett.3c01004>

### Author Contributions

<sup>‡</sup>Y.Z. and T.Z. contributed equally.

### Notes

The authors declare no competing financial interest.

## ■ ACKNOWLEDGMENTS

A.C. and J.W.C acknowledge the support from the Swiss National Science Foundation (SNF) (Sinergia, CRSIIS\_202296). J.W.C. acknowledges support from the National Research Foundation of Korea (NRF) (grants N R F - 2 0 2 1 R 1 A 2 B 5 B 0 3 0 0 1 9 5 6 a n d N R F - 2023M3H4A6A01058126) and the Technology Innovation Program (20012341) funded by the Ministry of Trade, Industry & Energy (MOTIE) of Korea, and generous support from the Institute of Engineering Research (IOER) and Research Institute of Advanced Materials (RIAM) at Seoul National University.

## ■ REFERENCES

- (1) Lin, D.; Liu, Y.; Cui, Y. Reviving the lithium metal anode for high-energy batteries. *Nat. Nanotechnol.* **2017**, *12* (3), 194–206.
- (2) Yang, X.-G.; Liu, T.; Wang, C.-Y. Thermally modulated lithium iron phosphate batteries for mass-market electric vehicles. *Nat. Energy* **2021**, *6* (2), 176–185.
- (3) Schmuck, R.; Wagner, R.; Höpfl, G.; Placke, T.; Winter, M. Performance and cost of materials for lithium-based rechargeable automotive batteries. *Nat. Energy* **2018**, *3* (4), 267–278.
- (4) Liu, J.; Bao, Z.; Cui, Y.; Dufek, E. J.; Goodenough, J. B.; Khalifah, P.; Li, Q.; Liaw, B. Y.; Liu, P.; Manthiram, A.; et al. Pathways for practical high-energy long-cycling lithium metal batteries. *Nat. Energy* **2019**, *4* (3), 180–186.
- (5) Zhang, X.; Yang, Y.; Zhou, Z. Towards practical lithium-metal anodes. *Chem. Soc. Rev.* **2020**, *49* (10), 3040–3071.
- (6) Choi, J. W.; Aurbach, D. Promise and reality of post-lithium-ion batteries with high energy densities. *Nat. Rev. Mater.* **2016**, *1* (4), 16013.
- (7) Zhang, J. G.; Xu, W.; Xiao, J.; Cao, X.; Liu, J. Lithium Metal Anodes with Nonaqueous Electrolytes. *Chem. Rev.* **2020**, *120* (24), 13312–13348.
- (8) Zheng, X.; Huang, L.; Ye, X.; Zhang, J.; Min, F.; Luo, W.; Huang, Y. Critical effects of electrolyte recipes for Li and Na metal batteries. *Chem* **2021**, *7*, 2312–2346.
- (9) Cheng, X. B.; Zhang, R.; Zhao, C. Z.; Zhang, Q. Toward Safe Lithium Metal Anode in Rechargeable Batteries: A Review. *Chem. Rev.* **2017**, *117* (15), 10403–10473.
- (10) Wang, H.; Yu, Z.; Kong, X.; Kim, S. C.; Boyle, D. T.; Qin, J.; Bao, Z.; Cui, Y. Liquid electrolyte: The nexus of practical lithium metal batteries. *Joule* **2022**, *6* (3), 588–616.
- (11) Qian, J.; Henderson, W. A.; Xu, W.; Bhattacharya, P.; Engelhard, M.; Borodin, O.; Zhang, J. G. High rate and stable cycling of lithium metal anode. *Nat. Commun.* **2015**, *6*, 6362.
- (12) Jiao, S.; Ren, X.; Cao, R.; Engelhard, M. H.; Liu, Y.; Hu, D.; Mei, D.; Zheng, J.; Zhao, W.; Li, Q.; et al. Stable cycling of high-voltage lithium metal batteries in ether electrolytes. *Nat. Energy* **2018**, *3* (9), 739–746.
- (13) Peng, Z.; Cao, X.; Gao, P.; Jia, H.; Ren, X.; Roy, S.; Li, Z.; Zhu, Y.; Xie, W.; Liu, D.; et al. High-Power Lithium Metal Batteries Enabled by High-Concentration Acetonitrile-Based Electrolytes with Vinylene Carbonate Additive. *Adv. Funct. Mater.* **2020**, *30* (24), No. 2001285.
- (14) Suo, L.; Xue, W.; Gobet, M.; Greenbaum, S. G.; Wang, C.; Chen, Y.; Yang, W.; Li, Y.; Li, J. Fluorine-donating electrolytes enable highly reversible 5-V-class Li metal batteries. *Proc. Natl. Acad. Sci. U. S. A.* **2018**, *115* (6), 1156–1161.
- (15) Chen, Y.; Yu, Z.; Rudnicki, P.; Gong, H.; Huang, Z.; Kim, S. C.; Lai, J.-C.; Kong, X.; Qin, J.; Cui, Y.; et al. Steric Effect Tuned Ion Solvation Enabling Stable Cycling of High-Voltage Lithium Metal Battery. *J. Am. Chem. Soc.* **2021**, *143* (44), 18703–18713.
- (16) Cao, X.; Ren, X.; Zou, L.; Engelhard, M. H.; Huang, W.; Wang, H.; Matthews, B. E.; Lee, H.; Niu, C.; Arey, B. W.; et al. Monolithic solid-electrolyte interphases formed in fluorinated orthoformate-based electrolytes minimize Li depletion and pulverization. *Nat. Energy* **2019**, *4* (9), 796–805.
- (17) Ren, X.; Zou, L.; Cao, X.; Engelhard, M. H.; Liu, W.; Burton, S. D.; Lee, H.; Niu, C.; Matthews, B. E.; Zhu, Z.; et al. Enabling High-Voltage Lithium-Metal Batteries under Practical Conditions. *Joule* **2019**, *3* (7), 1662–1676.
- (18) Chen, S.; Zheng, J.; Yu, L.; Ren, X.; Engelhard, M. H.; Niu, C.; Lee, H.; Xu, W.; Xiao, J.; Liu, J.; et al. High-Efficiency Lithium Metal Batteries with Fire-Retardant Electrolytes. *Joule* **2018**, *2* (8), 1548–1558.
- (19) Chen, S.; Zheng, J.; Mei, D.; Han, K. S.; Engelhard, M. H.; Zhao, W.; Xu, W.; Liu, J.; Zhang, J. G. High-voltage lithium-metal batteries enabled by localized high-concentration electrolytes. *Adv. Mater.* **2018**, *30* (21), No. 1706102.
- (20) Cao, X.; Gao, P.; Ren, X.; Zou, L.; Engelhard, M. H.; Matthews, B. E.; Hu, J.; Niu, C.; Liu, D.; Arey, B. W.; et al. Effects of fluorinated solvents on electrolyte solvation structures and electrode/electrolyte interphases for lithium metal batteries. *Proc. Natl. Acad. Sci. U. S. A.* **2021**, *118* (9), No. e2020357118.

- (21) Ren, X.; Gao, P.; Zou, L.; Jiao, S.; Cao, X.; Zhang, X.; Jia, H.; Engelhard, M. H.; Matthews, B. E.; Wu, H.; et al. Role of inner solvation sheath within salt-solvent complexes in tailoring electrode/electrolyte interphases for lithium metal batteries. *Proc. Natl. Acad. Sci. U. S. A.* **2020**, *117* (46), 28603–28613.
- (22) Tan, L.; Chen, S.; Chen, Y.; Fan, J.; Ruan, D.; Nian, Q.; Chen, L.; Jiao, S.; Ren, X. Intrinsic Nonflammable Ether Electrolytes for Ultrahigh-Voltage Lithium Metal Batteries Enabled by Chlorine Functionality. *Angew. Chem., Int. Ed.* **2022**, *61* (32), No. e202203693.
- (23) Zhou, T. H.; Zhao, Y.; El Kazzi, M.; Choi, J. W.; Coskun, A. Stable Solid Electrolyte Interphase Formation Induced by Monoquat-Based Anchoring in Lithium Metal Batteries. *ACS Energy Lett.* **2021**, *6* (5), 1711–1718.
- (24) Kim, M. S.; Zhang, Z.; Rudnicki, P. E.; Yu, Z.; Wang, J.; Wang, H.; Oyakhire, S. T.; Chen, Y.; Kim, S. C.; Zhang, W.; et al. Suspension electrolyte with modified Li<sup>+</sup> solvation environment for lithium metal batteries. *Nat. Mater.* **2022**, *21* (4), 445–454.
- (25) Li, W.; Yao, H.; Yan, K.; Zheng, G.; Liang, Z.; Chiang, Y.-M.; Cui, Y. The synergistic effect of lithium polysulfide and lithium nitrate to prevent lithium dendrite growth. *Nat. Commun.* **2015**, *6*, 7436.
- (26) Wang, Q.; Yao, Z.; Zhao, C.; Verhallen, T.; Tabor, D. P.; Liu, M.; Ooms, F.; Kang, F.; Aspuru-Guzik, A.; Hu, Y.-S.; et al. Interface chemistry of an amide electrolyte for highly reversible lithium metal batteries. *Nat. Commun.* **2020**, *11*, 4188.
- (27) Holoubek, J.; Liu, H.; Wu, Z.; Yin, Y.; Xing, X.; Cai, G.; Yu, S.; Zhou, H.; Pascal, T. A.; Chen, Z.; Liu, P.; et al. Tailoring Electrolyte Solvation for Li Metal Batteries Cycled at Ultra-Low Temperature. *Nat. Energy* **2021**, *6*, 303–313.
- (28) Xue, W. J.; Huang, M. J.; Li, Y. T.; Zhu, Y. G.; Gao, R.; Xiao, X. H.; Zhang, W. X.; Li, S. P.; Xu, G. Y.; Yu, Y.; et al. Ultra-high-voltage Ni-rich layered cathodes in practical Li metal batteries enabled by a sulfonamide-based electrolyte. *Nat. Energy* **2021**, *6* (5), 495–505.
- (29) Yu, Z.; Wang, H.; Kong, X.; Huang, W.; Tsao, Y.; Mackanic, D. G.; Wang, K.; Wang, X.; Huang, W.; Choudhury, S.; et al. Molecular design for electrolyte solvents enabling energy-dense and long-cycling lithium metal batteries. *Nat. Energy* **2020**, *5* (7), 526–533.
- (30) Zhou, T.; Zhao, Y.; El Kazzi, M.; Choi, J. W.; Coskun, A. Integrated Ring-Chain Design of a New Fluorinated Ether Solvent for High-Voltage Lithium-Metal Batteries. *Angew. Chem., Int. Ed.* **2022**, *61* (19), No. e202115884.
- (31) Yu, Z.; Rudnicki, P. E.; Zhang, Z.; Huang, Z.; Celik, H.; Oyakhire, S. T.; Chen, Y.; Kong, X.; Kim, S. C.; Xiao, X.; et al. Rational solvent molecule tuning for high-performance lithium metal battery electrolytes. *Nat. Energy* **2022**, *7* (1), 94–106.
- (32) Liu, B.; Zhang, J. G.; Xu, W. Advancing Lithium Metal Batteries. *Joule* **2018**, *2* (5), 833–845.
- (33) Fang, C.; Wang, X.; Meng, Y. S. Key Issues Hindering a Practical Lithium-Metal Anode. *Trends Chem.* **2019**, *1* (2), 152–158.
- (34) Zhao, Q.; Liu, X.; Stalin, S.; Khan, K.; Archer, L. A. Solid-state polymer electrolytes with in-built fast interfacial transport for secondary lithium batteries. *Nat. Energy* **2019**, *4* (5), 365–373.
- (35) Liu, F. Q.; Wang, W. P.; Yin, Y. X.; Zhang, S. F.; Shi, J. L.; Wang, L.; Zhang, X. D.; Zheng, Y.; Zhou, J. J.; Li, L.; et al. Upgrading traditional liquid electrolyte via in situ gelation for future lithium metal batteries. *Sci. Adv.* **2018**, *4* (10), No. eaat5383.
- (36) Kaberov, L. I.; Verbraeken, B.; Riabtseva, A.; Brus, J.; Talmon, Y.; Stepanek, P.; Hoogenboom, R.; Filippov, S. K. Fluorinated 2-alkyl-2-oxazolines of high reactivity: Spacer-length-induced acceleration for cationic ring-opening polymerization as a basis for triphilic block copolymer synthesis. *ACS Macro Lett.* **2018**, *7* (1), 7–10.
- (37) Li, J.; Huo, F.; Chen, T.; Yan, H.; Yang, Y.; Zhang, S.; Chen, S. In-situ construction of stable cathode/Li interfaces simultaneously via different electron density azo compounds for solid-state lithium metal batteries. *Energy Storage Mater.* **2021**, *40*, 394–401.
- (38) Zhao, Y.; Zhou, T.; Ashirov, T.; Kazzi, M. E.; Cancellieri, C.; Jeurgens, L. P. H.; Choi, J. W.; Coskun, A. Fluorinated ether electrolyte with controlled solvation structure for high voltage lithium metal batteries. *Nat. Commun.* **2022**, *13* (1), 2575.
- (39) Peljo, P.; Girault, H. H. Electrochemical potential window of battery electrolytes: the HOMO–LUMO misconception. *Energy Environ. Sci.* **2018**, *11* (9), 2306–2309.
- (40) Diederichsen, K. M.; McShane, E. J.; McCloskey, B. D. Promising routes to a high Li<sup>+</sup> transference number electrolyte for lithium ion batteries. *ACS Energy Lett.* **2017**, *2* (11), 2563–2575.
- (41) Yamada, Y.; Furukawa, K.; Sodeyama, K.; Kikuchi, K.; Yaegashi, M.; Tateyama, Y.; Yamada, A. Unusual stability of acetonitrile-based superconcentrated electrolytes for fast-charging lithium-ion batteries. *J. Am. Chem. Soc.* **2014**, *136* (13), 5039–5046.
- (42) Kimura, K.; Motomatsu, J.; Tominaga, Y. Correlation between solvation structure and ion-conductive behavior of concentrated poly (ethylene carbonate)-based electrolytes. *J. Phys. Chem. C* **2016**, *120* (23), 12385–12391.
- (43) Li, T.; Zhang, X. Q.; Yao, N.; Yao, Y. X.; Hou, L. P.; Chen, X.; Zhou, M. Y.; Huang, J. Q.; Zhang, Q. Stable Anion-Derived Solid Electrolyte Interphase in Lithium Metal Batteries. *Angew. Chem.* **2021**, *133* (42), 22865–22869.
- (44) Wu, F.; Liu, N.; Chen, L.; Su, Y.; Tan, G.; Bao, L.; Zhang, Q.; Lu, Y.; Wang, J.; Chen, S.; Tan, J. Improving the reversibility of the H<sub>2</sub>-H<sub>3</sub> phase transitions for layered Ni-rich oxide cathode towards retarded structural transition and enhanced cycle stability. *Nano Energy* **2019**, *59*, 50–57.
- (45) Yang, J.; Liu, X.; Wang, Y.; Zhou, X.; Weng, L.; Liu, Y.; Ren, Y.; Zhao, C.; Dahbi, M.; Alami, J.; et al. Electrolytes Polymerization-Induced Cathode-Electrolyte-Interphase for High Voltage Lithium-Ion Batteries. *Adv. Energy Mater.* **2021**, *11* (39), No. 2101956.
- (46) Beyene, T. T.; Bezabih, H. K.; Weret, M. A.; Hagos, T. M.; Huang, C.-J.; Wang, C.-H.; Su, W.-N.; Dai, H.; Hwang, B.-J. Concentrated dual-salt electrolyte to stabilize Li metal and increase cycle life of anode free Li-metal batteries. *J. Electrochem. Soc.* **2019**, *166* (8), A1501.
- (47) Miao, R.; Yang, J.; Xu, Z.; Wang, J.; Nuli, Y.; Sun, L. A new ether-based electrolyte for dendrite-free lithium-metal based rechargeable batteries. *Sci. Rep.* **2016**, *6*, 21771.
- (48) Zhao, C. Z.; Zhao, Q.; Liu, X.; Zheng, J.; Stalin, S.; Zhang, Q.; Archer, L. A. Rechargeable lithium metal batteries with an in-built solid-state polymer electrolyte and a high voltage/loading Ni-rich layered cathode. *Adv. Mater.* **2020**, *32* (12), No. 1905629.
- (49) Tan, S.; Zhang, Z.; Li, Y.; Li, Y.; Zheng, J.; Zhou, Z.; Yang, Y. Tris (hexafluoro-iso-propyl) phosphate as an SEI-forming additive on improving the electrochemical performance of the Li [Li<sub>0.2</sub>Mn<sub>0.56</sub>Ni<sub>0.16</sub>Co<sub>0.08</sub>] O<sub>2</sub> cathode material. *J. Electrochem. Soc.* **2013**, *160* (2), A285.